



# Effect of 2 MeV Electron Irradiation on the Electronic Structure and Photoluminescence of SiC

Wenjing Chang<sup>1</sup> · Rongxing Cao<sup>2</sup> · Kejia Wang<sup>1</sup> · Yuxiong Xue<sup>2</sup> · Xianghua Zeng<sup>1,2</sup>

Received: 22 December 2023 / Accepted: 7 February 2024 / Published online: 4 March 2024  
© The Minerals, Metals & Materials Society 2024

## Abstract

Silicon carbide (SiC) with the advantages of high thermal conductivity and high breakdown field strength can meet the new requirements of modern electronic technology for harsh conditions. Focusing on the application of deep space exploration, the present work has explored the effects of 2-MeV electron irradiation on 4H-SiC with a fluence of  $7 \times 10^{12} \text{ cm}^{-2}$  and  $1 \times 10^{13} \text{ cm}^{-2}$ . The samples irradiated with 2-MeV electrons and  $1 \times 10^{13} \text{ cm}^{-2}$  fluence have a smaller full width at half-maximum (FWHM) in both x-ray diffraction (XRD) and Raman spectra, weaker defect luminescence intensity in photoluminescence (PL) spectra, and increased Si-C bond ratio in x-ray photoelectron spectroscopy (XPS). These demonstrated that the electron irradiation at 2 MeV with the fluence of  $1 \times 10^{13} \text{ cm}^{-2}$  has caused the crystallization performance to recover in comparison with the original sample. The improved crystal quality can be ascribed to the thermal effects produced during the electron irradiation.

**Keywords** SiC single crystal · electron irradiation · irradiation effect

## Introduction

SiC has excellent optical, physical, and electronic properties with a wide band gap, high thermal conductivity, high electron saturation rate, large breakdown electric field, and good chemical stability. SiC also has a strong resistance to radiation, hence it is regarded as one of the best candidates for applications in a space irradiation environment.<sup>1</sup> Under the conditions of particle radiation in space, we need irradiation-resistant electronic components, therefore, it is a requisite task to study the effect of SiC materials irradiated by protons.

In a strong irradiation environment, particles colliding with atoms in the crystal lattice will result in the creation of defects within the crystal. These defects, along with the inherent defects of the crystal itself, will inevitably affect the

crystal quality of the SiC material, resulting in the degradation of the performance of devices based on the material. Hence, the reliability and durability of devices operating in a strong radiation environment degrade. Compared with proton and neutron irradiation, the effects of electron irradiation is moderate,<sup>2</sup> because most of the energy is lost in the interaction with the crystal electrons. Therefore, the use of electron irradiation to simulate the study of SiC materials in a space irradiation environment can show the microscopic effects of irradiation on materials more subtly.

Research on irradiation of 4H-SiC has attracted great attention. For example, Yang et al.<sup>3</sup> explored the anisotropy of defects by irradiating *n*-type 4H-SiC in different directions, and concluded that the interstitial defects are mainly distributed in the normal (0004) plane, and that the vacancy carbon antisite defects are mainly distributed in the transverse (11  $\bar{2}$  0) and (10  $\bar{1}$  0) crystal planes. Yu et al.<sup>4</sup> studied the influence of irradiation temperature on defects by using continuous and intermittent beam irradiation to control the temperature, and found that the irradiation under high temperature can produce thermal effects to repair defects. Kozlovski et al.<sup>5</sup> studied the defects at different temperatures (20, 200°C) and found that the number of defects generated under higher temperature is lower than that of low temperature.

✉ Yuxiong Xue  
yxxue@yzu.edu.cn

✉ Xianghua Zeng  
xhzeng@yzu.edu.cn; 815680487@qq.com

<sup>1</sup> College of Physics Science and Technology, Yangzhou University, Yangzhou 225002, China

<sup>2</sup> College of Electrical, Energy and Power Engineering, Yangzhou University, Yangzhou 225127, People's Republic of China

Although there have been some studies on electron irradiation of 4H-SiC, few studies on high-energy (2 MeV) electron irradiation at fluences of  $7 \times 10^{12} \text{ cm}^{-2}$  and  $1 \times 10^{13} \text{ cm}^{-2}$  have been reported. Therefore, in this paper, we have carried out experiments of 4H-SiC electron irradiation to study the changes of defects by means of x-ray diffraction (XRD; D8 Advance, Bruker), Raman (Renishaw inVia laser confocal Raman spectrometer), photoluminescence (PL; F-4700 FL; Hitachi), and x-ray photoelectron spectroscopy (XPS; ESCALAB250Xi) characterization. We found that, after electron irradiation of the 4H-SiC at 2 MeV and  $1 \times 10^{13} \text{ cm}^{-2}$ , the sample has better crystallization due to the thermal annealing effect caused by the electron irradiation.

## Experimental

### Test Sample

The *n*-type 4H-SiC single crystal used with a surface (0001) crystal plane was prepared by a physical vapor transport (PVT) method, purchased from PrMat. The sample size was

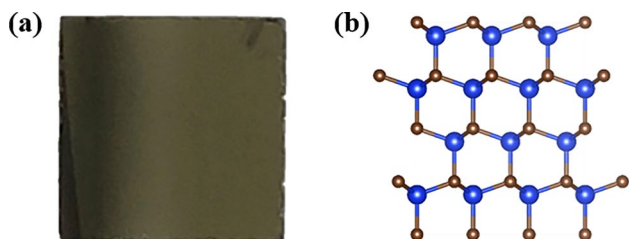


**Fig. 1** (a) Single-crystal sample of 4H-SiC; (b) cell structure of 4H-SiC.

5 mm × 5 mm with a thickness of 0.33 mm; both the sample and its cell structure are shown in Fig. 1a, b. Electron irradiation tests were carried out with 4H-SiC powders obtained by grinding single-crystal 4H-SiC into powder. The powders were irradiated with electrons of energy 2 MeV and fluences of  $7 \times 10^{12} \text{ cm}^{-2}$  and  $1 \times 10^{13} \text{ cm}^{-2}$ , and are labeled as samples #P1 and #P2, respectively. The pristine sample is labeled #P0.

The phase analysis of the samples was obtained by sampling XRD patterns under Cu K $\alpha$  ( $\lambda = 1.54 \text{ \AA}$ ) radiation. The Raman test was performed at 532 nm and the XPS measurements were acquired using a monochromatic Al K $\alpha$  x-ray source having a photon energy of 1486.7 eV, while the changes of the chemical bonds in the samples were observed. PL measurements were carried out at room temperature in order to determine the evolution of internal defects of the 4H-SiC before and after irradiation.

## Results and Discussion

### XRD Analysis

We performed XRD measurements of the samples before and after electron irradiation, as shown in Fig. 2a. First, we presented the patterns of the pristine 4H-SiC, where the diffraction peaks can be well matched with the structure of 4H-SiC (JCPDS No. 29-1127). Also, there is no appearance of other stray peaks, indicating that the crystals prepared by means of PVT have a good growth quality. Figure 2b shows the XRD patterns at  $2\theta = 33 - 39^\circ$ , and, since the three samples all exhibit better crystallization properties on the (102) crystal plane, taking the XRD pattern at  $2\theta = 38.15^\circ$  of (102) plane as an example, one can find that the main peak of  $38.02^\circ$  of #P0 shifts slightly to

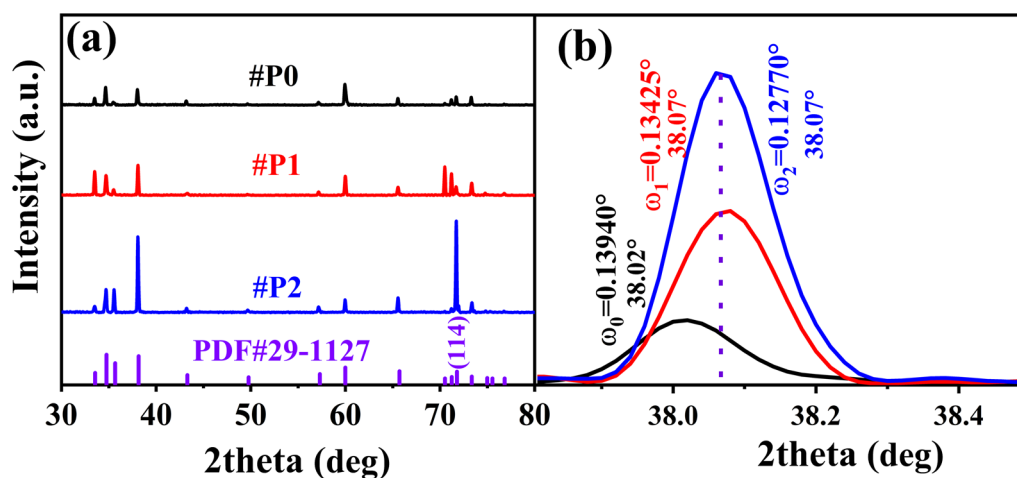


**Fig. 2** (a) XRD full spectrum, (b) (102) plane local magnification spectrum.

the lower angle of  $38.07^\circ$ , which is due to the displacement of the atoms in the sample by electron irradiation, resulting in lattice distortion. Table I shows the full width at half-maximum (FWHM) of the (102) crystal faces calculated by Gaussian fitting, FWHM is inversely proportional to the crystal quality and the grain size. Therefore, the smaller the FWHM, the better the crystal quality.<sup>6</sup> Sample #P2 has the smallest FWHM, which can be explained as the annealing effects induced by the electron irradiation. Specifically, during the irradiation process, the surface temperature of the sample increases due to the bombardment of high-energy particles, which makes some defects in the original sample recover and improves the crystal performance. With the increase of irradiation fluence, the rate of defect generation exceeds the rate of defect recovery by the annealing effect, so the FWHM of the (102) decreases from 0.139 to 0.127 for the three samples, that is, the crystal quality improves.

### Raman Analysis

Figure 3a shows the Raman spectra before and after electron irradiation at 2 MeV energy. As shown in Fig. 3a, no other obvious characteristic peaks appeared after the electron irradiation on the 4H-SiC, indicating that the irradiation at a certain injection amount did not result in a wide range of aberrations or recrystallization of the sample's crystal

structure, which is in agreement with the XRD results. 4H-SiC is a brazincite structure with eight atoms in its protocell and four vibrational modes ( $A_1 + B_1 + E_1 + E_2$ ); from the selection rule of Raman scattering, it can be seen that  $A_1$ ,  $E_1$  and  $E_2$  are Raman active and  $B_1$  is not Raman active. As shown in Fig. 3a, the Raman peaks at 240, 776, 981, and  $1525\text{ cm}^{-1}$  correspond to the transverse acoustic mode  $E_2(\text{TA})$ , the transverse optical mode  $E_2(\text{TO})$ , the longitudinal optical mode  $A_1(\text{LO})$ , and the optical branch, respectively.<sup>7–9</sup> Among these, the optical mode represents the relative motion of the atoms within the 4H-SiC protocell and the acoustic mode is the overall movement. It can be seen that in the range of  $100\text{--}550\text{ cm}^{-1}$  is the vibrational region of chemically bonded Si-Si, in the range of  $580\text{--}1000\text{ cm}^{-1}$  is the Si-C vibrational region, and in the range of  $1080\text{--}1600\text{ cm}^{-1}$  is the C-C vibrational region.

As  $776\text{ cm}^{-1}$  is the dominant peak of 4H-SiC, the displacement of the TO phonon mode is closely related to the compressive and tensile stress,<sup>10</sup> and the magnified spectrum at  $776\text{ cm}^{-1}$  is shown in Fig. 3b.  $E_2(\text{TO})$  values and their FWHM have been calculated by using Gaussian fitting, as displayed in Table II. Therefore, the smaller the FWHM, the better the crystallization performance of the crystal. The FWHM is equal to 5.063, 4.978, and  $4.895$  for the samples #P0, #P1 and #P2, respectively. One can find that, under the electron irradiation with a fluence of  $7 \times 10^{12}\text{ cm}^{-2}$ , 4H-SiC has a better crystal quality. As sample #P2 has the smallest FWHM, this means that the crystal of 4H-SiC is further improved after 2-MeV electron irradiation with  $1 \times 10^{13}\text{ cm}^{-2}$ .

Also, at this injection, the characteristic peak of  $E_2(\text{TO})$  shifted from  $775.66\text{ cm}^{-1}$  (#P0) to  $776.10\text{ cm}^{-1}$  (#P1), indicating that there has been the generation of compressive strain that makes the lattice distortion

**Table I** FWHMs at the (102) plane for the three samples.

Samples	FWHM
#P0	$0.13940 \pm 0.00226$
#P1	$0.13425 \pm 0.00142$
#P2	$0.12770 \pm 0.00181$

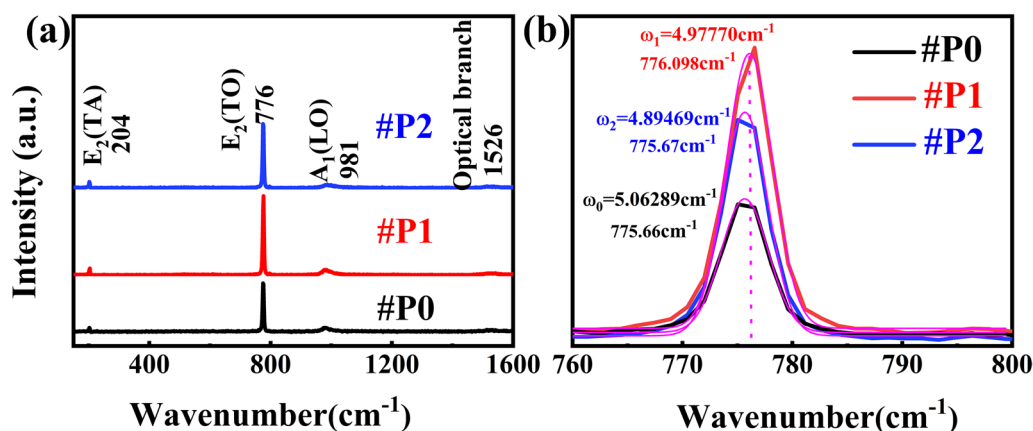


**Fig. 3** (a) Raman spectra; (b)  $760\text{--}800\text{ cm}^{-1}$  local magnification spectra.

produce lattice stress.<sup>11</sup> However, with the increase of irradiation fluence, the compressive strain of sample #P2 at  $775.67\text{ cm}^{-1}$  is weakened, that is, some defects that lead to compressive strain of the crystal are reduced. In addition, we fitted the overall Raman spectra before and after irradiation, and found that the area ratio of  $E_2$  (TO) in the overall Raman diffraction peak increases, as shown in Table II. The intensity of the Raman diffraction peak is related to the vibration of the chemical bond. In general, only heteronuclear bonds (C-Si bonds) are present in idealized SiC, and the presence of homonuclear bonds (C-C bonds, Si-Si bonds) implies a change in the lattice structure of electron-irradiated 4H-SiC, that is to say, the larger the proportion of C-Si bond, the better the crystal quality. Then, we can conclude that sample #P2 has more Si-C states, that is, the sample has better quality after irradiation.<sup>12</sup>

## PL Spectra

We have performed PL measurements of 4H-SiC before and after electron irradiation, as shown in Fig. 4a. The emission around 384 nm corresponds to the intrinsic emission peak of 4H-SiC, and the peak near 390 nm is the near band emission of 4H-SiC.<sup>13</sup> Sample #P0 has a weaker peak

intensity at 384 nm than that of samples #P1 and #P2. The weaker intensity is from the existence of the point defect, which interacts with the impurity atoms inside SiC to produce composite defects to capture exciton luminescence and suppress the intrinsic luminescence peak near the conduction band. To facilitate a better comparison of the intensity changes between the three peaks, the PL spectra have been rescaled based on the emission peaks at  $\sim 390\text{ nm}$ , as displayed in Fig. 4b. The emission from 500 nm to 750 nm is related to the defects in the SiC, hence the stronger PL peak corresponds to the larger defect density.<sup>14</sup> As observed in Fig. 4b, the ratio of defect intensity from sample #P2 is significantly lower than that of sample #P0, that is, the internal defects of sample #P2 are reduced after irradiation.

To study the defect behavior, two peaks of  $\sim 400\text{ nm}$  and  $\sim 540\text{ nm}$  were fitted with the Gaussian function, as shown in Fig. 5a and b, respectively, and the fitting results are displayed in Table III. The peak at  $\sim 400\text{ nm}$  can be deconvolved with two peaks 390 (or 391) and 384 (or 385) nm, as shown in Fig. 5a. Thus, we can conclude that the 2-MeV electron irradiation has almost no effect on the band gap of 4H-SiC.

The peak around 435 nm involves donor–acceptor pair recombination related to nitrogen (N) impurities.<sup>15</sup> The emission peaks located around  $\sim 526\text{ nm}$  and  $\sim 577\text{ nm}$  are ascribed to the  $(V_c + V_{si})$  carbon–silicon vacancy pair defects.<sup>16,17</sup> After irradiation, the luminescence peaks at 435 nm and 526–577 nm showed a decreasing trend, and it is speculated that the reduction of N-related defects is mainly the result of irradiation-induced  $(V_c + V_{si})$  deep defects. These deep defects interact with the inevitable N impurities introduced during the growth process, thereby reducing the presence of N impurities. In addition, the decrease in  $(V_c + V_{si})$  defects may also be due to the self-annealing characteristics of the defect states induced by the high-energy electron irradiation or by the outward migration of defect

**Table II**  $E_2$  (TO) and FWHM for the three samples

Samples	$E_2$ (TO) ( $\text{cm}^{-1}$ )	FWHM ( $\text{cm}^{-1}$ )	Ratio of $776\text{ cm}^{-1}$ (%)
#P0	775.66	$5.02689 \pm 0.09137$	55.85
#P1	776.10	$4.97770 \pm 0.09417$	58.45
#P2	775.67	$4.89469 \pm 0.08998$	59.43

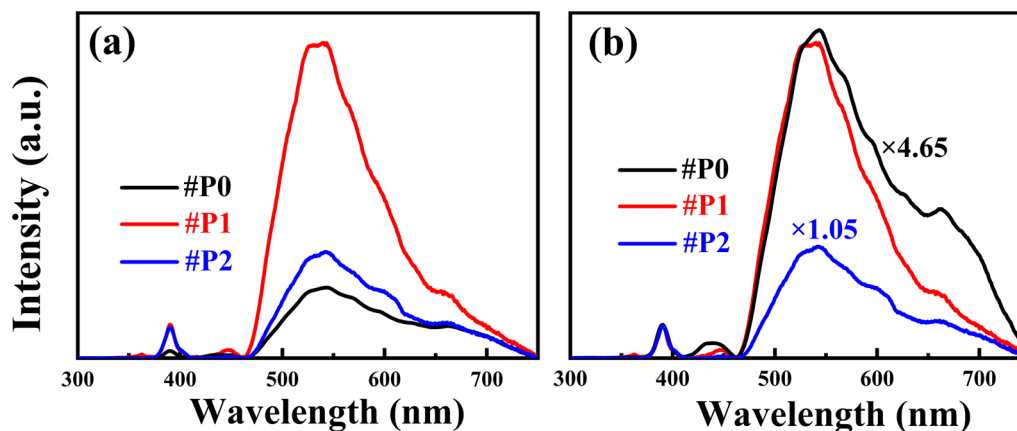


**Fig. 4** (a) PL spectra for the three samples; (b) rescaled PL spectra based on near band emission.

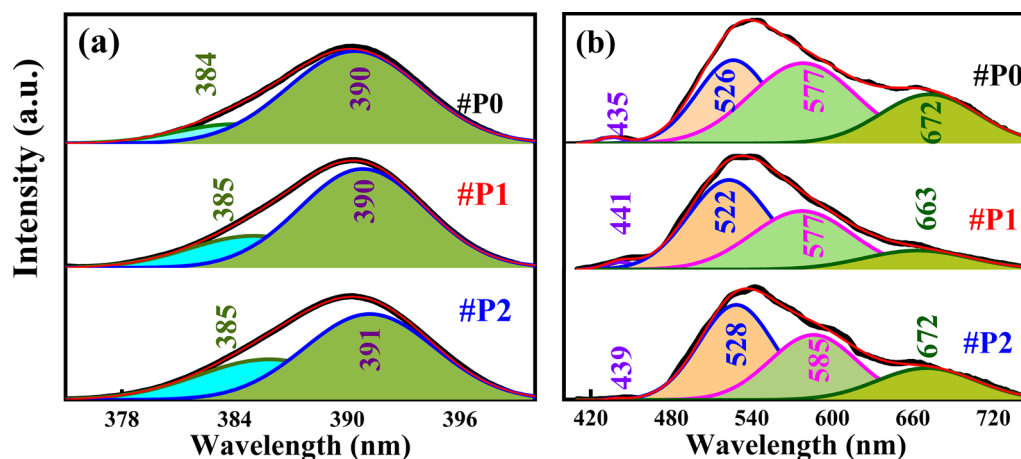


Fig. 5 PL spectra and their deconvolved peaks (a) from 350 nm to 410 nm and (b) from 410 to 730 nm.

Table III PL peaks for the three samples

Sample	$\lambda$ (nm)	E (eV)	Intensity ratio (%)	Defects <sup>14, 15, 16, 18</sup>
#P0	384	3.20	0.09	Intrinsic
	390	3.17	0.54	Band-edge
	435	2.85	0.82	N
	526	2.36	30.97	$V_c + V_{si}$
	577	2.15	43.56	$V_c + V_{si}$
	672	1.85	24.11	Si Frenkel
#P1	385	3.22	0.16	Intrinsic
	390	3.17	0.49	Band-edge
	441	2.81	1.43	N
	522	2.38	47.10	$V_c + V_{si}$
	577	2.15	37.90	$V_c + V_{si}$
	663	1.87	12.90	Si Frenkel
#P2	385	3.22	0.64	Intrinsic
	391	3.17	1.25	Band-edge
	439	2.82	0.15	N
	528	2.35	43.16	$V_c + V_{si}$
	585	2.12	35.11	$V_c + V_{si}$
	672	1.85	19.24	Si Frenkel

states in SiC.<sup>18</sup> The emission located at  $\sim 672$  nm corresponds to the Si Frenkel defects. Steeds et al. found that the defect can be annealed at a lower temperature.<sup>19</sup> Therefore, the weakening emission at  $\sim 672$  nm can be explained as the irradiation annealing effect.

Table III shows the possible defect recombination luminescence and the proportion of each luminescence peak in the sample corresponding to the luminescence peak obtained by Gaussian processing of the fitted 4H-SiC. For the three

samples, ( $V_c + V_{si}$ ) double-vacancy defects dominate, while for #P0, the intensity ratio of ( $V_c + V_{si}$ ) double-vacancy defects is 74.53 %, and is 85 % for #P1 and 78.27 % for #P2. Compared with #P1 and #P2, sample #P0 has a relatively lower ( $V_c + V_{si}$ ) double-vacancy defect but has higher Si Frenkel defect, as displayed in Table III.

### XPS Analysis

We performed XPS measurements on the samples, and the full XPS spectra are shown in Fig. 6. Four obvious peaks can be observed, which correspond to the three elements of Si, C, and O in all the samples. According to the full spectrum of #P0, the surface of the 4H-SiC single-crystal sample is very clean, there are almost no other impurities, and the elemental composition is consistent with the expected results.<sup>20,21</sup>

In order to more accurately analyze the chemical bonds, the XPS spectra of C 1s and Si 2p and their deconvoluted peaks were obtained, as displayed in Table IV. Figure 7 shows the C 1s and Si 2p spectra and their fittings. In Fig. 7a, for sample #P0, four peaks at 282.6, 284.6, 286.31, and 284.80 eV can be observed, which correspond to the binding states of the C-Si, C-C, C-O, and C-N bonds, respectively.<sup>22,23</sup> As shown in Fig. 7b, Si 2p can be well fitted with two peaks (100.34 and 100.91 eV) for sample #P0, which correspond to the bonding states of the Si-Si and Si-N bonds,<sup>24</sup> respectively.

As the relative atomic concentration in the sample is proportional to the peak intensity of the characteristic peak, the relative atomic content can be judged from the integrated peak area.<sup>25</sup> As shown in Table IV, in consideration of the Si-C bonds in the C1s orbital and the Si 2p

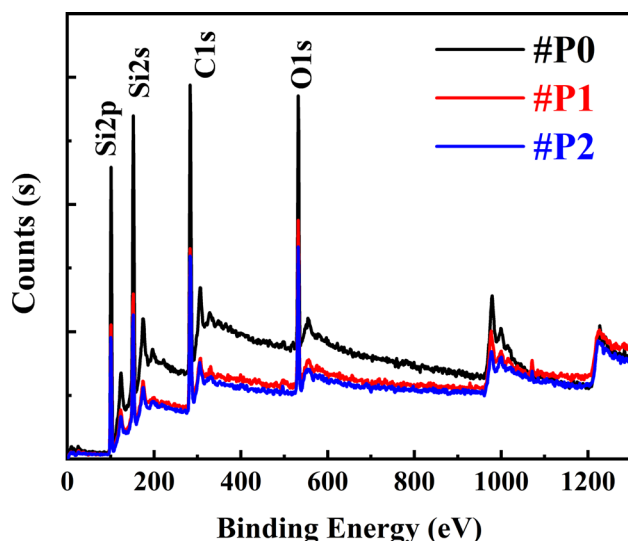


Fig. 6 XPS full spectra.

**Table IV** C 1s and Si 2p spectra and their deconvoluted peaks for the three samples

Samples	Spin orbital	Center/eV	FWHM	Ratio%	Chemical bond <sup>21, 22, 23</sup>
#P0	C1s	282.60	0.99	20.64	C-Si
		284.80	1.23	60.38	C-C
		286.31	1.30	13.88	C-O
		288.85	0.95	5.10	C-N
#P1	C1s	282.64	1.12	55.74	C-Si
		284.76	1.38	32.33	C-C
		286.25	1.69	10.37	C-O
		288.91	0.91	1.57	C-N
#P2	C1s	282.68	0.97	50.43	C-Si
		284.76	1.26	39.34	C-C
		286.24	1.41	8.77	C-O
		288.96	0.93	1.45	C-N
#P0	Si2p	100.34	1.11	79.61	Si-C
		100.91	0.93	20.39	Si-N
#P1	Si2p	100.53	1.33	79.74	Si-C
		101.56	2.93	20.26	Si-N
#P2	Si2p	100.51	1.24	84.93	Si-C
		102.05	3.43	15.07	Si-N

orbital, the proportion of the Si-C bond area in #P1 and #P2 has increased in comparison with #P0. In #P0, the ratio of the Si-C bond to other chemical bonds is about 1:1, while, in #P1 and #P2, the ratio of the Si-C bond to other chemical bonds is about 2:1. In general, only

heteronuclear bonds (C-Si bonds) are present in idealized SiC, and the presence of homonuclear bonds (C-C bonds, Si-Si bonds) implies a change in the lattice structure of the electron-irradiated 4H-SiC, that is to say, the larger the proportion of C-Si bond, the better the crystal quality, which further verifies that the 2-MeV electron irradiation can restore the crystallization performance of the sample. Combined with XRD and Raman analysis, the increase of the Si-C bond ratio is due to the irradiation annealing. Compared with #P0, the chemical bonds related to impurities such as C-O, C-N and Si-N bonds in #P1 and #P2 showed an overall decreasing trend, that is, the above defects were reduced under irradiation.

Furthermore, each individual peak has different degrees of chemical shift after irradiation, the main chemical shifts being for the two chemical bonds, C-C bond and C-Si bond, in C 1s which are shown in Fig. 7a. After electron irradiation, the C-Si bond shifts to the high binding energy (BE) direction and the C-C bond shifts to the low BE direction. In the study of Vali et al.<sup>21</sup>, the XPS spectra for the irradiated samples also showed the same phenomenon, which they explained as the irradiation effect and gas pollution in the air. Combined with the analysis in this paper, it may be that more Si dangling bonds are generated during the irradiation process. As shown in Fig. 7b, the two peaks of the Si 2p orbital have a tendency to shift to the high BE direction after irradiation.

## Conclusions

Electron irradiation at 2 MeV on 4H-SiC with a fluence of  $7 \times 10^{12} \text{ cm}^{-2}$  and  $1 \times 10^{13} \text{ cm}^{-2}$  has been studied. Some results have been obtained from the measurements of XRD, Raman, PL, and XPS spectra showing that, under the electron irradiation with a fluence of  $1 \times 10^{13} \text{ cm}^{-2}$ , the sample revealed an improved crystal quality, a decreased defect emission intensity, and an increased Si-C bond. Also, the obvious displacement damage observed at a fluence of  $7 \times 10^{12} \text{ cm}^{-2}$  is weakened at a fluence of  $1 \times 10^{13} \text{ cm}^{-2}$ . Therefore, we can conclude that the crystallinity of 4H-SiC has been improved after 2-MeV electron irradiation at a fluence of  $1 \times 10^{13} \text{ cm}^{-2}$ . The results are consistent with the reports<sup>4</sup> in which the improved crystal quality was ascribed to the stronger thermal effects of irradiation-repaired defects. These studies will be helpful in understanding the electron irradiation effects of 4H-SiC, to better serve deep space exploration.

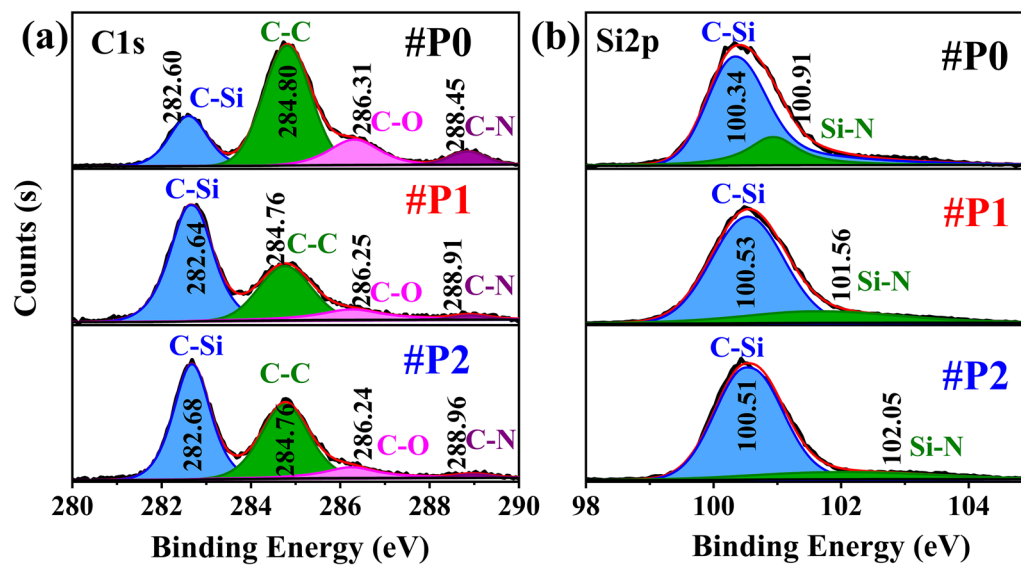


Fig. 7 XPS spectra of 4H-SiC (a) C1s and (b) Si2p.

**Acknowledgments** This work was supported by National Natural Science Foundation of China (12004329); Yangzhou Science and Technology Bureau, China (No. YZ2020263).

**Conflict of interest** The authors declare no competing financial interest.

## References

- S. Nigam, F. Jihyun Kim, G.Y. Ren, M.F. Chung, R. MacMillan, T.N. Dwivedi, R. Fogarty, K.K. Wilkins, C.R. Allums, S.J. Abernathy, J.R. Pearton, and Williams, High energy proton irradiation effects on SiC Schottky rectifiers. *Appl. Phys. Lett.* 81(13), 2385–2387 (2002).
- C. Kasper, D. Klenkert, Z. Shang, D. Simin, A. Gottscholl, A. Sperlich, H. Kraus, C. Schneider, S. Zhou, M. Trupke, W. Kada, T. Ohshima, V. Dyakonov, and G.V. Astakhov, Influence of irradiation on defect spin coherence in silicon carbide. *Phys. Rev. Appl.* 13, 044054 (2020).
- B. Yang, Y.K. Nakagawa, M. Kondo, and T. Shibayama, Anisotropic defect distribution in He<sup>+</sup>-irradiated 4H-SiC: effect of stress on defect distribution. *Acta Mater.* 211, 116845 (2021).
- B.W. Yu, Z. Wang, Y. Ma, N. Yang, X.Y. Deng, R. Guo, M.J. Xiang, M. Gong, Z.M. Yang, Y. Li, J.E. Li, X.L. Li, and Y. Feng, The radiation effects on 4H-SiC epilayers using different electron radiation methods. *Micro Nanostruct.* 166, 207216 (2022).
- V.V. Kozlovski, A.E. Vasil'ev, A.A. Lebedev, K.S. Davydovskaya, and M.E. Levinshtein, Effect of the electron-irradiation temperature on the formation of radiation defects in silicon carbide. *J. Surf. Invest.* 17(2), 397–400 (2023).
- S.C. Zhang, X.H. Cui, H.F. Liu, Y. Yang, H.Y. Chen, X. Li, D.F. Liu, and F. Zhu, Investigation of the recovery process in low-dose neutron-irradiated 6H-SiC by lattice parameter and FWHM of diffraction peak measurements. *Radiat. Effects Defects Solids* 177(7–8), 800–813 (2022).
- Y. Han, B.S. Li, Z.G. Wang, J.X. Peng, J.R. Sun, K.F. Wei, C.F. Yao, N. Gao, X. Gao, and L.L. Pang, H-ion irradiation-induced annealing in He-ion implanted 4H-SiC. *Chin. Phys. Lett.* 34, 012801 (2017).
- J.C. Burton, L. Sun, F.H. Long, Z.C. Feng, and I.T. Ferguson, First- and second-order Raman scattering from semi-insulating 4H-SiC. *Phys. Rev. B* 59, 7282 (1999).
- S. Nakashima and H. Harima, Raman investigation of SiC polytypes. *Phys. Stat. Sol. A* 162, 39 (1997).
- M. Yamamoto, M. Deki, T. Takahashi, T. Tomita, T. Okada, S. Matsuo, S. Hashimoto, M. Yamaguchi, K. Nakagawa, N. Uehara, and M. Kamano, Raman spectroscopic stress evaluation of femto-second-laser-modified region inside 4H-SiC. *Appl. Phys. Express* 3, 016603 (2010).
- S. Yang, S. Tokunaga, M. Kondo, Y. Nakagawa, and T. Shibayama, Non-destructive evaluation of the strain distribution in selected-area He<sup>+</sup> ion irradiated 4H-SiC. *Appl. Surf. Sci.* 500, 144051 (2020).
- N. Sreelakshmi, S. Amirthapandian, G.R. Umapathy, C. David, S.K. Srivastava, S. Ojha, and B.K. Panigrahi, Raman scattering investigations on disorder and recovery induced by low and high energy ion irradiation on 3C-SiC. *Mater. Sci. Eng. B* 273, 115452 (2021).
- I. Shalish, I.B. Altfeder, and V. Narayanamurti, Observations of conduction-band structure of 4H- and 6H-SiC. *Phys. Rev. B* 65, 073104 (2002).
- I.P. Vali, P.K. Shetty, M.G. Mahesha, V.C. Petwal, J. Dwivedi, D.M. Phase, and R.J. Choudary, Structural and optical studies of gamma irradiated N-doped 4H-SiC. *Nucl. Inst. Meth. Phys. Res. B* 440, 101–106 (2019).
- Y. Wu, L.F. Ji, Z.Y. Lin, Y.J. Jiang, and T.R. Zhai, Blue photoluminescence enhancement in laser-irradiated 6H-SiC at room temperature. *Appl. Phys. Lett.* 104, 041906 (2014).
- A. Castaldini, A. Cavallini, L. Rigutti, N. Filippo, F. Sergio, and G. Fabrizio, Deep levels by proton and electron irradiation in 4H-SiC. *J. Appl. Phys.* 98, 053706 (2005).
- A. Castaldini, A. Cavallini, and L. Rigutti, Assessment of the intrinsic nature of deep level Z1/Z2 by compensation effects in proton-irradiated 4H-SiC. *Semicond. Sci. Technol.* 21, 724 (2006).

18. J.W. Steeds, W. Sullivan, A. Wotherspoon, and J.M. Hayes, Long-range migration of intrinsic defects during irradiation or implantation. *J. Phys. Condens. Matter* 21, 364219 (2009).
19. J.W. Steeds and A. Sarua, Photoluminescence evidence for silicon Frenkel defects in electron irradiated 4H-SiC. *AIP Adv.* 13, 045016 (2023).
20. W. Jiang, Y. Zhang, M.H. Engelhard, W.J. Weber, and G.J. Exarhos, Behavior of Si and C atoms in ion amorphized SiC. *J. Appl. Phys.* 101, 023524 (2007).
21. B.J. Wang, J.H. Yin, D.H. Chen, X.J. Long, L. Li, H.H. Lin, W.G. Hu, D.N. Talwar, R.X. Jia, Y.M. Zhang, I.T. Ferguson, W.H. Sun, Z.C. Feng, and L.Y. Wan, Optical and surface properties of 3C-SiC thin epitaxial films grown at different temperatures on 4H-SiC substrates. *Superlattices Microstruct.* 156, 106960 (2021).
22. I.P. Vali, P.K. Shetty, M.G. Mahesha, V.C. Petwal, J. Dwivedi, D.M. Phase, and R.J. Choudhary, Electron and gamma irradiation effects on Al/n-4H-SiC Schottky contacts. *Vacuum* 172, 109068 (2020).
23. E. Velez-Fort, C. Mathieu, E. Pallecchi, M. Pigneur, M.G. Silly, R. Belkhou, M. Marangolo, A. Shukla, F. Sirotti, and A. Ouerghi, Epitaxial graphene on 4H-SiC (0001) grown under nitrogen flux: evidence of low nitrogen doping and high charge transfer. *ACS Nano* 6, 10893–10900 (2012).
24. T. Tanaka, M. Takizawa, and A. Hata, Verification of the effectiveness of UV-polishing for 4H-SiC wafer using photocatalyst and cathion. *Int. J. Autom. Technol.* 12(2), 160–169 (2018).
25. H. Shimada, N. Matsubayashi, M. Imamura, T. Sato, and A. Nishijima, XPS depth profiling by changing incident X-ray energy. *Appl. Surf. Sci.* 100–101, 56–59 (1996).

**Publisher's Note** Springer Nature remains neutral with regard to jurisdictional claims in published maps and institutional affiliations.

Springer Nature or its licensor (e.g. a society or other partner) holds exclusive rights to this article under a publishing agreement with the author(s) or other rightsholder(s); author self-archiving of the accepted manuscript version of this article is solely governed by the terms of such publishing agreement and applicable law.